DFT-based spectral moments estimators for spaceborne Doppler precipitation radar

Simone Tanelli*[a], Eastwood Im[a], Luca Facheris[b], Eric A. Smith[c]

[a] Jet Propulsion Laboratory, California Institute of Technology, Pasadena CA, USA
[b] Dipartimento di Elettronica e Telecomunicazioni, Università di Firenze, Firenze, Italy
[c] NASA/Goddard Space Flight Center, Greenbelt MD, USA

ABSTRACT

In this paper an in-depth analysis on the performance of the Fourier analysis in estimating the first spectral moment of Doppler spectra of rain signals from a spaceborne radar is presented. The spectral moment estimators based on the Fourier analysis (DFT-SME) have been widely used in the field of Doppler weather radar in measuring rainfall velocity and they have been found to be almost optimal for small normalized spectral widths (w_N). They are also more computationally efficient than the Maximum Likelihood estimators. However, the existing analytical approaches for evaluating the DFT-SME performance have mostly been focused on a limited range of small w_N (*e.g.*, $w_N < 0.1$) that are typical of ground based and airborne Doppler weather radars. With the rapid advances in spaceborne radar technologies, the flying of a Doppler precipitation radar in space to acquire global data sets of vertical rainfall velocity has become a real possibility. The objective of this work is to develop a generalized analytical approach such that it can be extended to larger values of w_N (*e.g.*, $w_N \sim 0.2$) in spaceborne radar applications. In particular, a method has been developed to properly treat the aliasing effects, which have become a significant error source in spaceborne remote sensing. Furthermore, several versions of DFT-SME (differing on the adopted strategies for noise handling and choice of the first guess of the mean Doppler velocity) have been analyzed with this generalized approach. The analytical results are in excellent agreement with those obtained through simulation. Such encouraging results suggest that the proposed approach is a reliable technique for fast and accurate prediction of DFT-SME performance for a variety of spaceborne radar system parameters.

Keywords: Spaceborne weather radar, Doppler, DFT, Spectral moments estimation

1. INTRODUCTION

The research to assess the performances of spectral moments estimators (SME) applied to Doppler weather radars has been focusing so far to the class of 'narrow spectra'[1]. Although the boundary of such class cannot be defined in strict terms, a qualitative classification based on the applicability of the various approximations assumed in such performance assessments can be as follows: when the normalized spectral width $w_N < 0.1$ the effects of aliasing can be neglected with no significant loss of validity of the results, in this case all conclusions drawn for narrow spectra hold satisfactorily. Ground-based and airborne Doppler weather radars developed in the last decades were designed to provide spectral widths in this range[1,2,3,4]. On the other hand, when $w_N > 0.3$ the spectrum can be undoubtedly classified as 'broad' and SME performances (which can be rated in general as 'poor') are to be evaluated following more complex approaches. In the region between 0.1 and 0.3, the properties and approximate formulas used for narrow spectra loose (progressively when increasing w_N) their validity, therefore more accurate approaches are necessary to accurately assess the performances of a SME.

When spaceborne applications of Doppler weather radar are considered, relatively large normalized spectral widths (w_N) are to be foreseen. In fact, if the antenna pattern can be approximated by a 2-D Gaussian, the w_N of the Doppler spectrum measured by a pulsed weather radar observing a spatially homogeneous random field can be expressed as[4]:

$$w_N = \frac{2}{\lambda}\frac{1}{PRF}\sqrt{w_R^2 + \frac{\theta_{3dB}^2 v_S^2}{16\ln(2)}} \tag{1}$$

*Simone Tanelli, Jet Propulsion Laboratory, M.S. 300-243 4800 Oak Grove Drive, Pasadena, CA 91109, U.S.A. E-mail: simone@radar-sci.jpl.nasa.gov

where λ is the operating wavelength, *PRF* is the Pulse Repetition Frequency, v_s its linear velocity, and θ_{3dB} is the antenna 3dB width (one way), w_R is the Doppler spectral width of the distributed target (in the case of rainfall w_R ranges between 1 and 5 m/s). For a Low Earth Orbiting satellite v_s is typically ~7 km s^{-1}. Furthermore we can consider the approximation $\theta_{3dB} \cong \gamma \lambda / D$, where γ can be typically assumed ~1.25, it follows from Eq. (1) that w_N does not depend significantly on λ. The PRF upper bound is determined mainly by the thickness of the atmosphere layer to be monitored: for precipitation measurements at a scanning angle β we have:

PRF \ D [m]	2	3	4	5	6	10
5000	0.50	0.34	0.25	0.20	0.17	0.10
6000	0.42	0.28	0.21	0.17	0.14	0.09
7000	0.36	0.24	0.18	0.14	0.12	0.07
8000	0.32	0.21	0.16	0.13	0.11	0.06

Table (1): Normalized spectral widths w_N as function of (*PRF* and antenna diameter D) for v_s = 7000 m s^{-1}.

$$PRF < \frac{c}{2H} \frac{1}{\cos(\beta)} \tag{2}$$

where H is the troposphere thickness (typically around 20 km) and c is the speed of light. Depending on the scanning strategy (*i.e.*, maximum β) we can consider a maximum PRF ranging between 5000 Hz and 8000Hz. Table 1 shows the normalized spectral widths for different spaceborne radar configurations.

While an antenna of 10m could provide spectra with w_N similar to that of airborne radars, obvious economical and technological requirements lead to the choice of smaller antennas, whenever possible. On the other hand, a 2 m antenna such as that of the TRMM Precipitation Radar (PR) or the one planned for the dual frequency precipitation radar of the GPM mission, even if a nadir-only scanning strategy is considered (i.e., the only one allowing PRF up to 8 kHz) would generate spectra with $w_N > 0.3$, unsuitable for accurate estimates of any spectral moment. Antenna diameters between 3 and 6 meters are therefore considered as the region where to look for the optimal trade-off, for the purpose of radar system and mission design. The corresponding range of w_N is between 0.1 and 0.3.

In Section 2 the Discrete Fourier Transform based SME (DFT-SME, elsewhere referred to also as *periodogram processing*) is described, in Section 3 the method for DFT-SME performance assessment is described and, finally, in Section 4 results of such method are compared with those provided by previously developed methods and with simulations.

2. RAINFALL DOPPLER SPECTRUM AND DFT-SME

Let us consider the sequence of *M* complex radar samples $\tilde{s}_n = s_n + n_n$ spaced by T_S=*1/PRF* and affected by rainfall signal fluctuation[6] and white noise. The estimate of the power spectrum *P(f)* is given by[1]:

$$\tilde{P}(f) = \frac{1}{M} \left| \sum_{n=0}^{M-1} \tilde{s}_n \cdot e^{-2\pi j f T_S n} \right|^2 \tag{3}$$

Such estimate is calculated in discrete-time / discrete-frequency through the Fast Fourier Transform, or, more generally, by the Discrete Fourier Transform:

$$\tilde{P}_k = \frac{1}{M} \left| \sum_{n=0}^{M-1} \tilde{s}_n \cdot e^{-2\pi j k n / M} \right|^2 \quad \text{for } k=-M/2, \ldots, M/2-1 \tag{4}$$

In general we are interested in the zero-th moment (related to the rain reflectivity), in the first moment (related to the rainfall average vertical velocity) and in the second order central moment (related to the rainfall Doppler width, and therefore to the spread of raindrop diameters around the mean diameter). When a narrow spectrum is observed, the Pulse Pair algorithm (PP) was proved to be the most efficient SME [7] (in fact it does not require the calculation of the whole spectrum, and therefore it requires the minimum amount of calculations, it reaches the theoretical optimum performance

given by the Cramer-Rao bound, is not significantly affected by aliasing and it is not biased by white noise). However, PP performances quickly degrade by increasing w_N. Recent studies [5] show that already for $w_N \sim 0.17$ the DFT-SME performs better than PP thanks to the lower sensitivity that DFT-SME has towards w_N. Furthermore, the DFT-SME is more versatile when the Gaussian shape of the Doppler spectrum cannot be granted (such as is the case when Non Uniform Beam Filling occurs [5]).

The DFT-SME algorithm can be implemented in several ways differing from each other for the noise handling approach, and the aliasing handling approach. As observed by Sirmans and Bumgardner [8] the different approach adopted when implementing DFT-SME can affect significantly the expected performances.

The mean velocity estimate through DFT technique can be expressed as:

$$\hat{v} = -\frac{\lambda}{2MT_S} m_0 = -\frac{\lambda}{2MT_S}\left\{ m_0' + \frac{1}{(S_S + S_N) - \hat{S}_N} \sum_{m=m_0'-M/2}^{m_0'+M/2} (m - m_0') \cdot \left[(S_{\mathrm{mod}_M(m)} + N_{\mathrm{mod}_M(m)}) - \hat{N}_{\mathrm{mod}_M(m)} \right] \right\} \qquad (5)$$

where S_S and S_N are the signal and noise power, respectively, while $\hat{S}_N$ is the estimated mean noise power and m_0' is an index corresponding to a first guess approximation α of the mean spectral frequency (i.e., $m'_0 = . \alpha M / PRF$.

The Doppler spectral width instead is calculated as follows:

$$\hat{w} = -\frac{\lambda}{2MT_S}\left\{ \frac{1}{(S_S + S_N) - \hat{S}_N} \sum_{m=m_0-M/2}^{m_0+M/2} (m - m_0)^2 \cdot \left[(S_{\mathrm{mod}_M(m)} + N_{\mathrm{mod}_M(m)}) - \hat{N}_{\mathrm{mod}_M(m)} \right] \right\}^{1/2} \qquad (6)$$

The first issue pertinent to the use of this technique is the approach to determine the initial guess index m_0'. The simplest approach is to assume $m_0'=0$. Three DFT-SME based on this approach are analyzed in [8], they differ in terms of noise handling as follows: a first method (DFT-Z) does not remove any white noise contribution (i.e., $\hat{S}_N = 0$ in Eqs. (5) and (6)). A second method (DFT-ZN) removes the nominal power (i.e., $\hat{S}_N = S_N$) in order to eliminate the bias due to white noise. A third method (DFT-ZT) cuts off all spectral lines with power density below a fixed threshold from the maximum. As shown in that paper, all of these approaches are very sensitive to the noise level: DFT-Z shows the smallest standard deviations $\sigma(v)$ but it is also significantly biased when $v \neq 0$ and SNR < 20dB, DFT-ZN instead is unbiased but its $\sigma(v)$ at low SNR's are significantly degraded, DFT-ZT shows a behavior between the former two approaches.

An unbiased version of DFT-Z was suggested by Zrnic [7]: when the Doppler spectrum is narrow (e.g.,$w_N < 0.1$) and M is large (e.g., $M>1000$), m_0' can be chosen equal to the index of the sample with the largest power. That is, $m_0' : \tilde{P}_{m_0'} = \max\{\tilde{P}_k\}$. This version will be referred to as DFT-M. For the spaceborne radar configuration in this study, however, neither of these two conditions applies. In fact besides the limitations on w_N discussed in Section 1, also the integration time $T_I = M\,T_S$ undergoes more stringent limitations than it would in the case of ground-based or airborne systems. This is due to the high antenna velocity (which sets issues of stationarity of the observed process [5] and of scanning strategy). In practice M ranging between 32 and 512 can be adopted for spaceborne applications.

Recently, a two-step DFT approach (DFT-I) was devised which provides more stable estimates for spaceborne applications. In the first step, Eq. (5) is applied with $m_0' = 0$ and the first velocity guess $\hat{v}^{(1)}$ is obtained. In the second step, the m_0' is set equal to $\hat{v}^{(1)}/(-\lambda/2MT_S)$ and a new estimate is obtained. This second step is iterated until the estimate converges: in fact, it can be easily verified that Eq. (5) can be reduced to:

$$\hat{v} = \hat{v}^{(1)} + \mathrm{sgn}(\hat{v}^{(1)}) \cdot \frac{\lambda}{2T_S} \frac{1}{(S_S + S_N) - \hat{S}_N} \left\{ \sum_{m=m_1^{(1)}}^{m_2^{(1)}} \left[(S_{\mathrm{mod}_M(m)} + N_{\mathrm{mod}_M(m)}) - \hat{N}_{\mathrm{mod}_M(m)} \right] \right\} \qquad (7)$$

where $m_1^{(1)}=u(-m_0')-sgn(-m_0')M/2$ and $m_2^{(1)}=u(m_0')-sgn(-m_0')M/2$. It follows that every further iteration of the second step requires only 1 real multiplication and less than M real sums. This does not change appreciably the computational efficiency of the SME-DFT. In practice, the iteration is stopped when the difference between the final estimate and the initial guess drops below the Doppler resolution $\lambda/(2MT_s)$.

3. DFT-SME PERFORMANCE ESTIMATION

Performance predictors of the DFT-Z have been derived by Berger and Groginsky [9], however these equations hold only for narrow and zero-centered spectra. In this work a more generalized approach which applies to a wider range of spectra is derived starting from the work of Miller and Rochwrger [10].

Let us define the aliased signal power spectrum $S_A(f)$ of the time windowed sequence:

$$S_A(f) = \sum_i S(f - i \cdot 2f_m) \otimes |D(f)|^2 \tag{8}$$

where $D(f)$ is the Fourier of the data window which is assumed unitary for convenience. The observed periodogram $\tilde{P}(f)$ is such that:

$$P(f) = \left\langle \tilde{P}(f) \right\rangle = S_A(f) + N(f) \tag{9}$$

where $< >$ indicates the expectation and $N(f) = S_N/2f_m$. The estimated signal power spectrum $\bar{S}(f)$ is therefore:

$$\bar{S}(f) = \left\langle \hat{S}(f) \right\rangle = P(f) - \hat{N}(f) \tag{10}$$

where $\hat{N}(f)$ is the estimated noise power spectrum.

Let:

$$M_{(k,\alpha)}[G(f)] = \int_{-f_m}^{f_m} f^k G(f+\alpha) df\,, \tag{11}$$

where α is the initial guess of the central frequency, and:

$$p(f) = \tilde{P}(f) - P(f) \tag{12}$$

Clearly $E<M_{(k,\alpha)}[p(f)]> = 0$ for any k and α. Therefore we have the following expression for the moments of the estimated signal periodogram:

$$m_{(k,\alpha)}[\hat{S}(f)] = \frac{M_{(k,\alpha)}[\hat{S}(f)]}{M_{(0,\alpha)}[\hat{S}(f)]} = \frac{M_{(k,\alpha)}[\bar{S}(f)] + M_{(k,\alpha)}[p(f)]}{M_{(0,\alpha)}[\bar{S}(f)] + M_{(0,\alpha)}[p(f)]} \tag{13}$$

which can be approximated at the second order of the expansion series for $M_{(0)}[p(f)]/M_{(0)}[S(f)] < 1$:

$$m_{(k,\alpha)}[\hat{S}(f)] = \left[M_{(k,\alpha)}(\bar{S}(f)) + M_{(k,\alpha)}(p(f))\right] \frac{1}{M_{(0)}(\bar{S}(f))} \left[1 - \frac{M_{(0)}(p(f))}{M_{(0)}(\bar{S}(f))} + \left(\frac{M_{(0)}(p(f))}{M_{(0)}(\bar{S}(f))}\right)^2\right] \tag{14}$$

A simpler expression can be obtained by omitting the high order terms $o(M^2_{(k,\alpha)}(p))$:

$$m_{(k,\alpha)}[\hat{S}] = \Psi_{k,\alpha} - \frac{1}{\hat{S}_S}\left[\Psi_{k,\alpha}\mu_0 - \mu_{k,\alpha}\right] + \frac{1}{\hat{S}_S^2}\left[\Psi_{k,\alpha}\mu_0^2 + \mu_0\mu_{k,\alpha}\right] \tag{15}$$

where, $\hat{S}_S = S_S + S_N - \hat{S}_N = M_{(0)}[\bar{S}(f)]$ and $\Psi_{k,\alpha} = M_{(k,\alpha)}[\bar{S}(f)]/\hat{S}_S$ are deterministic variables, while $\mu_{k,\alpha} = M_{(k,\alpha)}[p(f)]$ are zero-mean random variables.

3.1 Statistics of the first spectral moment estimator

The expectation of the estimator in Eq. (5) is obtained starting from Eq. (14) with $k=1$:

$$\left\langle \hat{f}_c \right\rangle = \alpha + \Psi_{1,\alpha} + \Xi_{1,\alpha} \tag{16}$$

where $\Xi_{1,\alpha}$ is the expected value of the contribution of the second order terms of Eq. (14) and can be expressed as:

$$\Xi_{1,\alpha} = -\frac{1}{MT_S}\frac{1}{\hat{S}_S^{\,2}}\int_{-f_m}^{f_m}(f-\Psi_{1,\alpha})P^2(f+\alpha)df \tag{17}$$

this expression is strictly valid only for $M \to \infty$, however it still holds if MT_s is significantly smaller than the spectral width.

Under the assumption that $w_N < 1/3$ the aliased spectrum can be well approximated by the terms in Eq. (7) with $i = -1,0,+1$:

$$S_A(f) = \sum_{i=-1}^{1}\frac{S_S}{\sqrt{2\pi}w}e^{-\frac{(f-(f_c+2if_m))^2}{2w^2}} \otimes \left|D(f)\right|^2 \tag{18}$$

in this case the integrals in Eqs. (16) and (17) can be solved analitically and the following expressions are obtained after removing a few negligible terms:

$$\Psi_{1,\alpha} = \frac{S_S}{\hat{S}_S}\left\{ f_{c,\alpha} + f_m\left[erf\left(\frac{f_m - f_{c,\alpha}}{\sqrt{2}w_D}\right) - erf\left(\frac{f_m + f_{c,\alpha}}{\sqrt{2}w_D}\right)\right]\right\} \tag{19}$$

where $f_{c,\alpha} = f_c - \alpha$, is the offset of the true central frequency from the first guess α and:

$$\begin{aligned}\Xi_{1,\alpha} = &\frac{1}{M}\frac{1}{\hat{S}_S^2}\frac{S_S^2 f_m}{2\sqrt{\pi}w_D}\left\{\left(\Psi_{1,\alpha} - f_{c,\alpha}\right) + f_m\left[erf\left(\frac{f_m + f_{c,\alpha}}{w_D}\right) - erf\left(\frac{f_m - f_{c,\alpha}}{w_D}\right)\right]\right\} + \\ &+\frac{1}{M}\frac{1}{\hat{S}_S^2}2S_N S_S\left\{\left(\Psi_{1,\alpha} - f_{c,\alpha}\right) + f_m\left[erf\left(\frac{f_m + f_{c,\alpha}}{\sqrt{2}w_D}\right) - erf\left(\frac{f_m - f_{c,\alpha}}{\sqrt{2}w_D}\right)\right]\right\}\end{aligned} \tag{20}$$

i	P_i	f_i	w_i
1	$\frac{S_S^2}{2\sqrt{\pi}w_D}$	$f_{c,\alpha}$	$w_D/\sqrt{2}$
2		$f_{c,\alpha}+2f_m$	
3		$f_{c,\alpha}-2f_m$	
4	$\frac{S_S S_N}{f_m}$	$f_{c,\alpha}$	w_D
5		$f_{c,\alpha}+2f_m$	
6		$f_{c,\alpha}-2f_m$	
7	$\frac{S_S^2}{\sqrt{\pi}w_D}e^{\frac{f_m^2}{w_D^2}}$	$f_{c,\alpha}+f_m$	$w_D/\sqrt{2}$
8		$f_{c,\alpha}-f_m$	

Table (2): Parameters to be used in Eq. (22) to get the expected standard deviation of the first moment estimates.

A simple analytical expression for the variance of the first moment estimator estimator can be obtained when $M_{(0)}[p(f)]/M_{(0)}[S(f)] \ll 1$. In this case, Eq.(14) can be truncated at the first order and one obtains:

$$\mathrm{var}(\hat{f}_c) = \left\langle \left(\hat{f}_c - \left\langle \hat{f}_c \right\rangle\right)^2 \right\rangle = \left\langle \frac{1}{\hat{S}_S^2}\left[\Psi_{1,\alpha}\mu_0 - \mu_{1,\alpha}\right]^2 \right\rangle \tag{21}$$

which can be rewritten, following the same considerations applied to Eq. (17), as:

$$\mathrm{var}\left(\hat{f}_c\right) = \frac{1}{MT_S}\frac{1}{\hat{S}_S^{\,2}}\int_{-f_m}^{f_m}(f-\Psi_{1,a})^2 P^2(f+\alpha)df \tag{22}$$

Once again, this expression can be solved analytically for a spectrum as in Eq. (18):

$$\mathrm{var}\left(\hat{f}_c\right)=\frac{1}{MT_S^2}\frac{1}{\hat{S}_S{}^2}\left[\frac{1}{12}S_N^2+\left(\frac{\Psi_{1,\alpha}}{2f_m}\right)^2 S_N^2+\right.$$
$$\left.+\sum_{i=1}^{9}\frac{P_i}{2f_m}\left\{\left[erf\left(\frac{f_m-f_i}{\sqrt{2}w_i}\right)-erf\left(\frac{-f_m-f_i}{\sqrt{2}w_i}\right)\right]\frac{w_i^2+\left(f_i-\Psi_{1,\alpha}\right)^2}{2}-\right.\right.$$
$$\left.\left.\frac{1}{\sqrt{2\pi}}w_i\left[e^{-\frac{(f_m-f_i)^2}{2\sigma_i^2}}(f_m-\Psi_{1,\alpha})-e^{-\frac{(f_m+f_i)^2}{2\sigma_i^2}}(-f_m-\Psi_{1,\alpha})\right]\right\}\right] \tag{23}$$

where the values of P_i , f_i and w_i are shown in Table 2. A more compact expression that holds for $w_N<0.2$ and $|f_{c,\alpha}|<f_m-1.7w_N$ can be obtained:

$$\mathrm{var}(\hat{V})=\frac{1}{MT_S^2}\frac{S_S^2}{\hat{S}_S^2}\left\{\left[\frac{w_N}{4\sqrt{\pi}}+2w_N^2\frac{S_N}{S_S}+\frac{1}{12}\left(\frac{S_N}{S_S}\right)^2\right]+\left[\frac{(f_{c,\alpha}-\Psi_{1,\alpha})^2}{2f_m}\left(\frac{1}{2\sqrt{\pi}w}+\frac{2}{f_m}\frac{S_N}{S_S}\right)+\left(\frac{\Psi_{1,\alpha}}{2f_m}\frac{S_N}{S_S}\right)^2\right]\right\} \tag{24}$$

where $w_N = w_D / 2f_m$ is the normalized spectral width. This expression matches exactely the well known result from Zrnic when $f_c = \alpha = 0$ and the noise power is precisely known. However, this equation shows also the dependence on the central frequency and on its first guess. It can be noted that if $f_{c,\alpha} << f_m$ then $\Psi_{I,\alpha}\cong f_{c,\alpha} S_S/ S_E$ and the second term in the right-hand side of Eq. (23) can be written as:

$$\frac{f_{c,\alpha}^2}{(2f_m)^2}\left[\frac{(S_N-\hat{S}_N)^2}{\hat{S}_S^2}\left(\frac{1}{2\sqrt{\pi}w_N}+2\frac{S_N}{S_S}\right)+\left(\frac{S_N}{\hat{S}_S}\right)^2\right] \tag{25}$$

which is useful to quickly evaluate the impact of $f_{c,\alpha}$ on the variance of the estimate when the spectrum is not affected by significan aliasing.

3.2 Statistics of the second spectral moment estimator

The statistics of the second central moment can be derived starting from Eq. (14):

$$\hat{w}_\alpha^2=m_{(2,\alpha)}[\hat{S}(f)]-\hat{f}_c^2=\Psi_{2,\alpha}-\Psi_{1,\alpha}^2-\frac{1}{\hat{S}_S}\left[\left(\Psi_{2,\alpha}-2\Psi_{1,\alpha}^2\right)\mu_0-2\Psi_{1,\alpha}\mu_{1,\alpha}-\mu_{2,\alpha}\right]+$$
$$+\frac{1}{\hat{S}_S^2}\left[\left(\Psi_{2,\alpha}-3\Psi_{1,\alpha}^2\right)\mu_0^2+\left(4\Psi_{1,\alpha}\mu_{1,\alpha}-\mu_{2,\alpha}\right)\mu_0-\mu_{1,\alpha}^2\right] \tag{26}$$

Analytic expressions for the bias and standard deviation of the second central moment can be derived from Eq. (25) following the same approach used in Section 3.1. However this paper does not focus on the estimation of the second spectral moment. In fact, it may be noted from Eq. (1) and (8) that the spectral width is mainly determined by the satellite motion and by the data window. In general, retrieval of rainfall parameters (such as spread of the terminal velocities due to drop size distribution and turbulence) from low earth orbiting satellites gives rise to several issues independent on the performance of the SME. For this reason this paper focuses on the estimation of the first spectral moment.

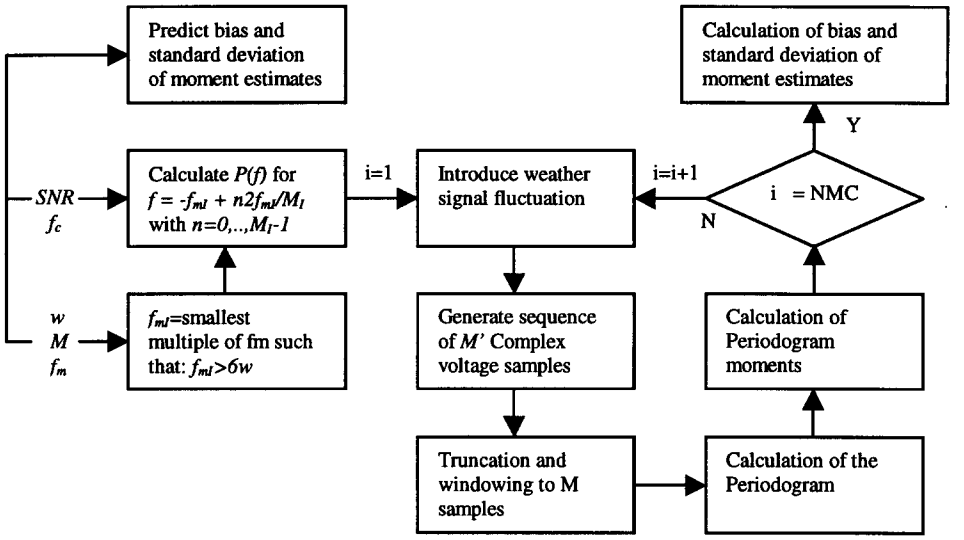

Fig. 1 Flow diagram of the simulations

3.3 Simulations

Weather spectra have been simulated for different f_c, w_N, *SNR* and M in order to a) verify the accuracy of the expressions obtained in Section 3.1 and b) compare the performances of the DFT-SME methods DFT-Z, DFT-ZN, DFT-M and DFT-I dicussed in Section 2.

As shown in Fig. 1 the simulation is divided in two phases: in the first phase the weather signal expected power spectrum is synthesized assuming an ideal Pulse Repetition Frequency (PRF_I) such that no aliasing occurs and a number of pulses M_I and such that the frequency resolution PRF_I/M_I << PRF/M. In the second phase, noise and random fluctuation are introduced and a corresponding 'ideal' sequence of M_I complex voltage samples separated by $1/PRF_I$ is generated as in [8]. The actual sequence of M complex voltage samples separated by 1/PRF is then obtained by downsampling and applying a data window to the 'ideal' sequence. The simulated periodograms are obtained through DFT processing of the actual sequence and their spectral moments are calculated through SME-DFT. The second phase is repeated *NMC* times (here *NMC* = 10000) to obtain several independent realizations and calculate bias and standard deviation of the estimated spectral moments.

4. Results

In this section the performances of DFT-Z, DFT-ZN, DFT-M and DFT-I in estimating the central frequency of the Doppler spectrum are analyzed and compared. For sake of generality all shown results refer to estimates of the normalized central frequency $f_N = f_c / PRF$. Furthermore the convention of showing the standard deviation $\sigma(f_N)=[var(f_N)]^{0.5}$ normalized by a factor $M^{0.5}$ is adopted for easiness of comparison with other studies available in literature. Although the linear dependence of $\sigma(f_N)$ on $M^{-0.5}$ (see section 3.1) is not strictly respected for DFT-M for the reasons discussed below, the quantity $M^{0.5}\,\sigma(f_N)$ is almost invariant with M.

Having focused this study on the effects of aliasing on the performances of DFT-SME, a parameter to quickly estimate the impact of aliasing was derived from Eq. (18):

$$\varepsilon_A = 0.5\left[1 - erf\left(\frac{0.5-|f_N|}{\sqrt{2}w_N}\right)\right] \tag{27}$$

A threshold at $\varepsilon_Q=0.05$ is used to define when significant aliasing occurs. The corresponding threshold in terms of f_N is $f_Q = 0.5 - 0.17w_N$.

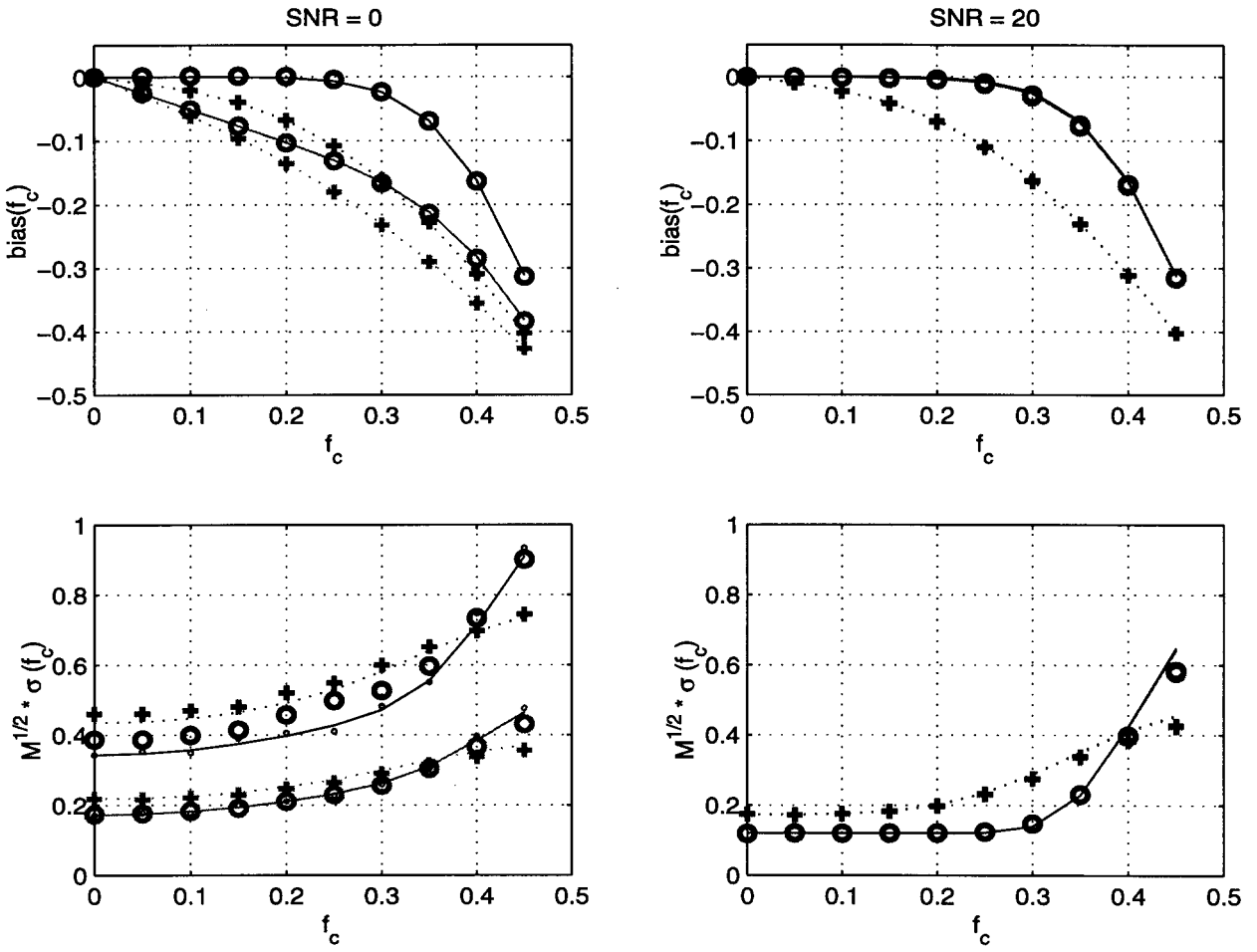

Fig. 2: Statistics of the estimates of the normalized central frequency f_c. Results of simulations with $M = 64$ are indicated by plus signs ($w_N = 0.1$) and large circles ($w_N = 0.2$), plot c also shows the standard deviation of DFT-ZN calculated from simulations with $M = 512$ (small circles). Values calculated through Eqs. (16) and (23) are shown with continuous lines ($w_N = 0.1$) and dotted lines ($w_N = 0.2$). Performances (both simulated and predicted) of DFT-Z are shown in grey and those of DFT-ZN are shown in black.

4.1 Performances of DFT-Z and DFT-ZN

The methods DFT-Z and DFT-ZN, first described in Section 2, are the simplest approaches to DFT-SME. It has been demonstrated [8] that their performances are equivalent for high SNR (i.e., SNR > 20dB), whereas for low SNR's, the former is biased towards zero and the latter shows significantly larger standard deviation of the estimate. These conclusions are confirmed by Figure 2 where the statistics of f_N estimates as obtained from DFT-Z (gray) and DFT-ZN (black) are shown for two levels of SNR, two spectral widths, and $0 \le f_N < 0.5$. Furthermore it can be noticed that the approach developed in Section 3.1 provides an extremely accurate assessment of $bias(f_N) = <\hat{f}_N> - f_N$ and standard deviation $\sigma(f_N)=[var(f_N)]^{0.5}$ for both methods. Figs 2c and 2d show that the observed standard deviations differ from the theoretically predicted values at low SNR and $M = 64$, in fact, in this case, the condition $M_{(0)}[p(f)]/M_{(0)}[S(f)] << 1$ is not verified and Eq. (12) is not accurately approximated by truncating at the first order the expansion series. The discrepancy disappears for $M = 512$ (small circles in Fig 2c), for higher SNR, and when the noise power is not removed as in method DFT-Z.

In general, the performances of both methods deteriorate proportionally to the aliased portion of the spectrum. This is evident for the bias shown in Fig. 3: in particular, for DFT-ZN, $\varepsilon_A \equiv |bias(f_N)|$.

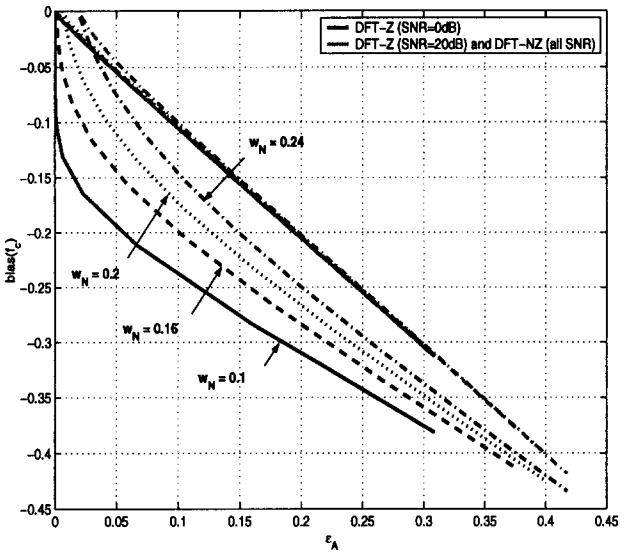

Fig. 3: Bias of DFT-Z and DFT-ZN vs. ε_A. Black lines of different styles indicate bias for DFT-Z at low SNR for different spectral widths. Bias for higher SNR and for DFT-ZN (all SNR's) are clustered around the $bias(f_N) = -\varepsilon_A$ line.

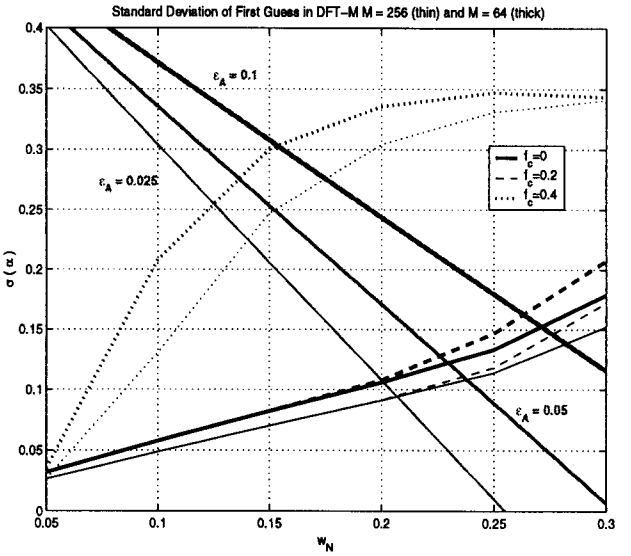

Fig. 4: Standard deviation of the first guess α obtained as in DFT-M (black) compared to the f_N corresponding to three ε_A values (grey). Thick black lines are obtained with M = 64, thin black lines are obtained with M = 256.

4.2 Performances of DFT-M

As discussed in Section 2, the DFT-M method aims at eliminating biases due to aliasing by initializing with a first guess of f_N. Such method is highly effective for large M (i.e., M =1024) and narrow spectra. Although its behavior cannot be predicted by the Perturbation Analysis [9], the results of simulations prove that it is practically unbiased for $\varepsilon_A < \varepsilon_Q$ (see Fig. 6b). However, Figs 4c and 4d show that the standard deviation of DFT-M estimates deteriorates, with respect to those from DFT-Z and DFT-ZN, for $w_N > 0.1$. This is due to the fact that the standard deviation of of the first guess α increases linearly with w_N. In Figure 4, $\sigma(\alpha)$ is compared to the offset of the center frequency that corresponds to mild ($\varepsilon_A = \varepsilon_Q/2$), significant ($\varepsilon_A = \varepsilon_Q$) and heavy ($\varepsilon_A = 2\varepsilon_Q$) aliasing, respectively. For instance, when $w_N = 0.2$ and M = 64,we have that $\sigma(\alpha)=\varepsilon_Q$ for low $|f_N|$. This means that the first guess removes all aliasing only 66% of the time. The dependence of $\sigma(\alpha)$ on f_c (see dash and dot lines) further increases this effect. Smaller $\sigma(\alpha)$ are obtained if larger M are used: it was observed that $\sigma(\alpha) \propto M^{-0.1}$ for $32 \leq M \leq 1024$.

4.3 Performances of DFT-I

Figures 5,6 and 7 provide a general comparison of the results of simulations for the four DFT methods discussed in this paper. While DFT-ZN rejects only the bias from white noise, DFT-M and DFT-I are able to reduce also the bias due to aliasing. In particular, the latter of the two maintains an acceptable bias rejection for a wider range of f_N than DFT-M.

The standard deviation of DFT-I is comparable to that of DFT-Z and that of DFT-ZN for all SNR and w_N and for a wide range of f_N. It can be noted, from Figs 6b and 6d, that DFT-I rejects the effects of aliasing better than the other methods by showing low bias and standard deviation for $\varepsilon_A < 0.15$, which corresponds to $f_N < 0.5 - w_N$. On the other hand, it is clear from Fig. 6d that when $\varepsilon_A > 0.1$ the standard deviation of DFT-I estimates rises rapidly above that of DFT-Z and DFT-M estimates. However, also in the region of high ε_A, DFT-I performances are still acceptable considering that in the same conditions DFT-Z and DFT-ZN are heavily biased and DFT-M shows an even higher standard deviation. Furthermore, Fig. 7 is useful to interpret correctly the statistics calculated for $\varepsilon_A > 0.1$. Fig 7a shows the standard deviation calculated for all methods and for two different f_N. For $f_N = 0$ (black lines in plots a and b) $\sigma(f_N)$ for DFT-M and DFT-I equals that of DFT-Z and DFT-ZN only for small w_N. In the region of wider spectra DFT-M and DFT-I show $\sigma(f_N)$ larger than DFT-Z and DFT-ZN, while DFT-Z and DFT-ZN are, in general, affected by a significant bias.

The effect of aliasing becomes more evident for $f_N = 0.4$. As shown in Fig. 7a, $\sigma(f_N)$ rises sharply around $w_N = 0.03$ for DFT-M and $w_N = 0.1$ for DFT-I. Above those thresholds $\sigma(f_N)$ reaches extremely high values and shows only little sensitivity to SNR (see gray lines in Fig 7b). This behaviour of $\sigma(f_N)$ is easily explained by observing the histograms in

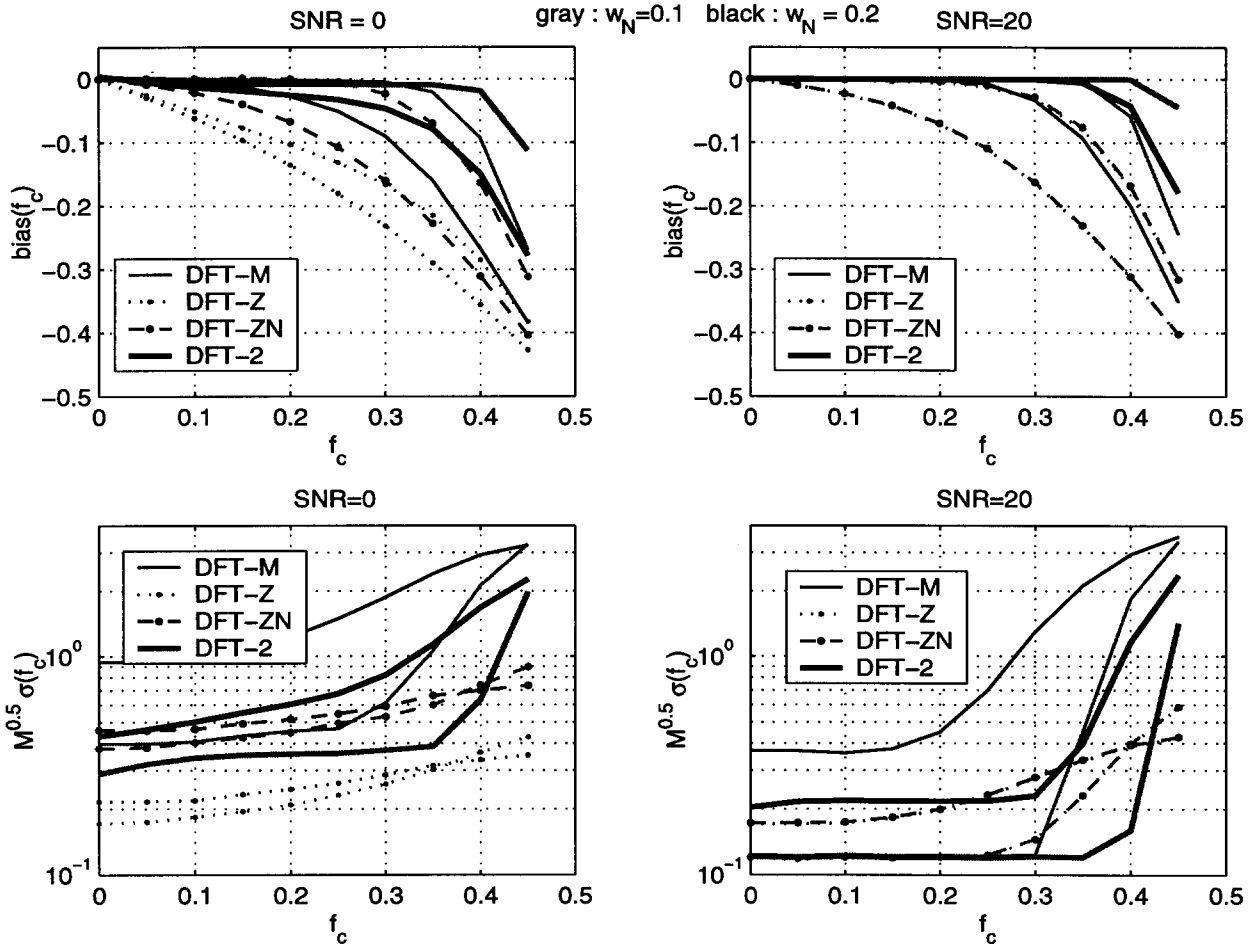

Fig 5: Comparison of bias (plots a and b) and standard deviation (plots c and d) of normalized central frequency estimates obtained with four DFT-SME approaches. All results are calculated from simulations with M = 64 and w_N = *0.1* (grey) or w_N = *0.2* (black).

Figs 7c and d: while the distribution of DFT-Z and DFT-ZN estimates are approximately Gaussian and significantly biased towards zero, DFT-M estimates are distributed accordingly to a bimodal distribution and also the distribution of DFT-I estimates shows secondary, weaker, modes. Note that the primary mode of the distribution is unbiased with respect to f_N. The 'bump' around the secondary modes (the aliased portion of the primary 'bump') appear because of the uncertainties on the fisrt guess estimates of f_N and could be corrected with more complex processing schemes. For DFT-I the secondary mode can be effectively removed by increasing M (e.g., for $f_N = 0.4$, $w_N = 0.2$ and $SNR = 20$, the secondary mode of DFT-I estimates disappears for $M > 128$), this is not true for DFT-M (due to the fact that $\sigma(\alpha) \propto M^{-0.1}$).

5. CONCLUSIONS

Use of spaceborne Doppler radars in low earth orbit to monitor the vertical velocity of rainfall requires the use of spectral moments estimators (SME) for spectra wider than those typically observed from ground-based and airborne Doppler precipitation radars. One of the most versatile family of spectral moment estimators (DFT-SME) is that based on the analysis of the whole spectrum obtained through Discrete Fourier Transform. However, the performances of such estimators vary considerably depending on the details of every specific approach. In this paper four approaches are studied, focusing on their performances in the intermediate range of normalized spectral widths w_N between 0.1 and 0.3.

A theoretical approach was developed to account for the effects of aliasing when deriving the bias and standard deviations of the estimates of the first spectral moment. The derived statistics are in excellent agreement with the results of simulations and they confirmed that the simplest 'zero-centered' approaches, namely DFT-Z and DFT-ZN, are not

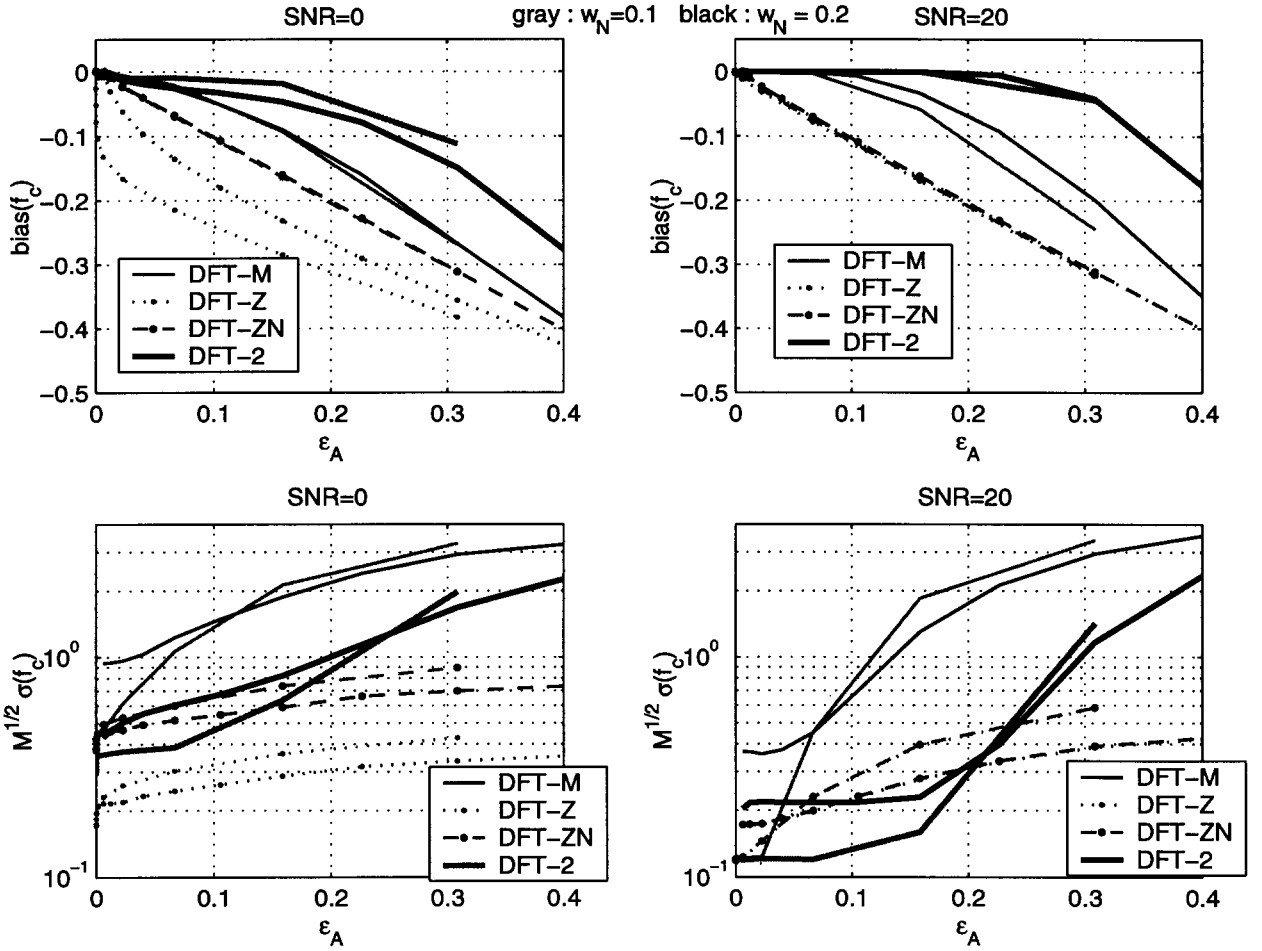

Fig 6: Comparison of bias (plots a and b) and standard deviation (plots c and d) of normalized central frequency estimates obtained with four DFT-SME approaches. All results are calculated from simulations with M = 64 and w_N = *0.1* (grey) or w_N = *0.2* (black). The parameter ε_A in abscissa is calculated through Eq. (27).

suited for applications with wide spectra: both show large biases when w_N = *0.2* even for small normalized central frequencies f_N and high SNR's.

Analysis of the statistics obtained through DFT-M revealed that also this approach, although effectively rejecting aliasing effects (and therefore providing unbiased estimates of f_N with small standard deviation) for narrow spectra, is not suited for estimating f_N of wide spectra. In particular, it has been observed that the standard deviation of f_N estimates is significantly larger than those of DFT-Z or DFT-ZN, and that the range of f_N that can be estimated with no bias is limited to a narrow region around zero. On the other hand, performances of DFT-I are overall satisfactory for wide spectra: estimates are basically unbiased (for high SNR's) and with standard deviations comparable to DFT-Z for a wide range of central frequencies (*i.e.*, $|f_N| < 0.5 - w_N$.). It is noted also that standard deviations of DFT-M and DFT-I estimates are not strictly proportional to $M^{-0.5}$ because of the methods to obtain the initial guess, therefore the results discussed in this paper, calculated for M = 64, are only indicative for very different values of M.

6. ACKNOWLEDGEMENT

The research described in this paper was based on the work performed for the TRMM follow-on programs at the Jet Propulsion Laboratory, California Institute of Technology, under contract with the National Aeronautics and Space Administration; at NASA Goddard Space Flight Center, and at the University of Florence (Italy) through a program funded by the Italian Space Agency.

REFERENCES

1. R.J. Doviak and Zrnic D.S., "Doppler radar and weather observations", *Academic Press*, 1984.
2 S.L. Durden, E. Im, F.K. Li, W. Ricketts, A. Tanner and W. Wilson, "ARMAR: An Airborne Rain-Mapping Radar". *J. Atmos. Oceanic Technol.*, **11**, pp. 727-737, 1994.
3 P.H. Hildebrand, C.A. Walther, C.L. Frush, J. Testud and F. Baudin, "The ELDORA/ASTRAIA Airborne Doppler Weather Radar: Goals, Design, and First Field Tests". *Proceedings of IEEE*, **82**, pp. 1873-1990, 1993.
4 G.M. Heymsfield et al., "The EDOP Radar System on the High-Altitude NASA ER-2 Aircraft", *J. Atmos. Oceanic Technol.*, **13**, 795-809, 1996.
5 S.Tanelli, E. Im, S.L.Durden, L. Facheris and D. Giuli, "The effects of nonuniform beam filling on vertical rainfall velocity measurements with a spaceborne Doppler radar". *J. Atmos. Oceanic Technol.*, **19**, pp. 1019-1034, 2001.
6. Marshall J.S. and Hitschfeld W., "Interpretation of the fluctuating Echo for randomly distributed scatterers. Part I", *Can. J. Phys.*, **31**, pp.962-995, 1953.
7. D.S. Zrnic', "Estimation of spectral moments for weather echoes", *IEEE Trans. On Geosc. Electr.*, **4**, pp.113-128, 1979.
8. D. Sirmans and B. Bumgarner, "Numerical comparison of five mean frequency estimators". *J. Appl. Meteor.*, **14**, 991-1003, 1975.
9. Berger T. and H.L. Groginsky, "Estimation of the spectral moments of pulse trains", presented at the *Int. Conf. On Inform. Theory*, Tel Aviv, Israel, 1973.
10. K. Miller and M.M. Rochwarger , "On estimating spectral moments in the presence of colored noise", *IEEE Trans. On Inf. Theory*. **16**, pp. 303-309, 1972.

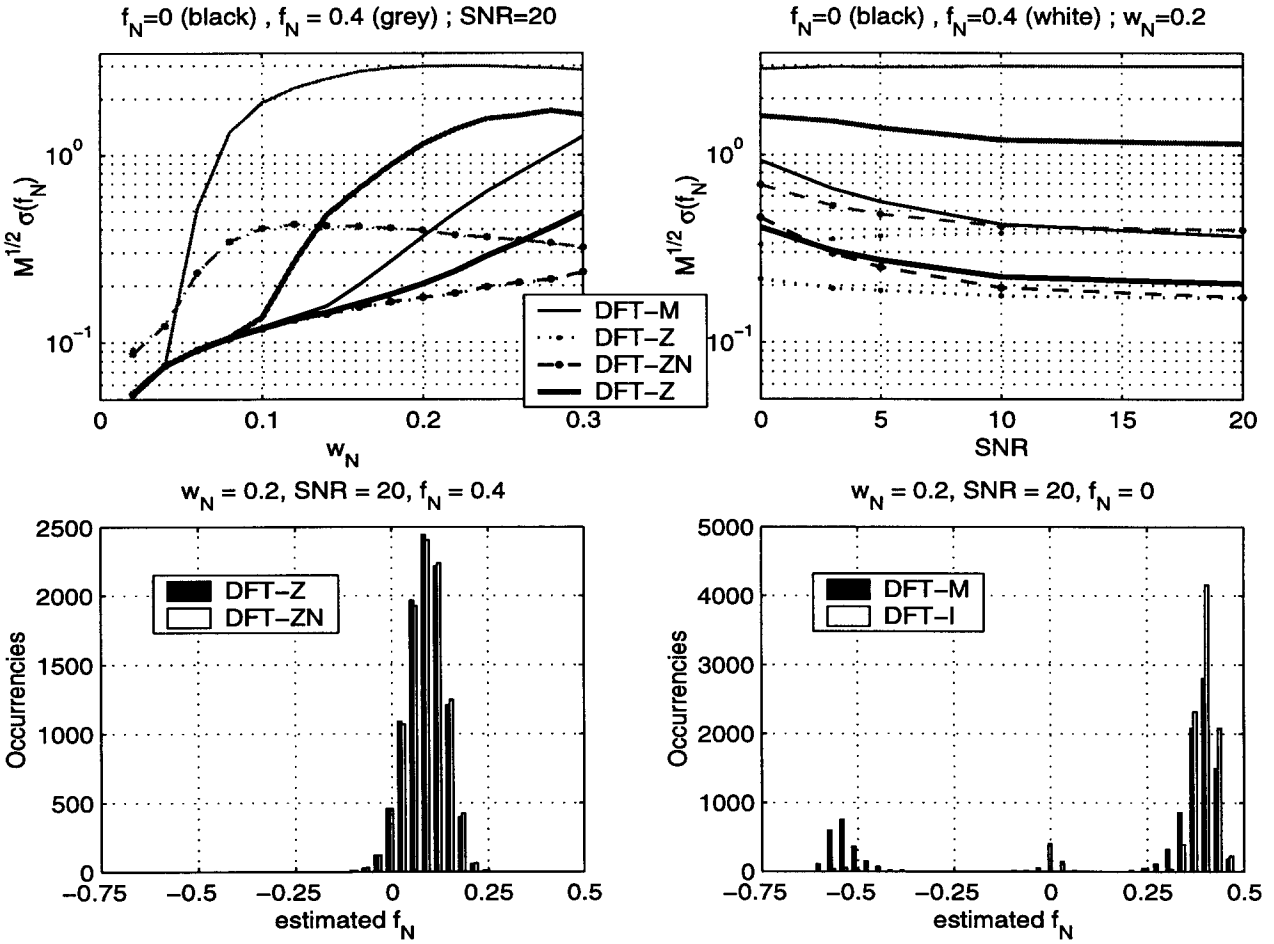

Fig 7: Effect of aliasing on f_N estimates by 4 SME-DFT approaches. Top: Normalized Standard deviation for $f_N = 0$ (black) and $f_N = 0.4$ (gray) vs. spectral width (a) and vs. SNR (b). Bottom: histograms of f_N estimates for $f_N = 0.4$, $w_N = 0.2$ and SNR = 20dB for 10000 realizations. Under these conditions the distribution of DFT-M estimates is bimodal, and that of DFT-I also shows a large tail, while that of DFT-Z and DFT-ZN is fairly Gaussian but heavily biased. The loss of Gaussian shape accounts for the sharp increase in DFT-M (at $w_N = 0.03$) and DFT-I (at $w_N = 0.1$) standard deviations in plot a) for $f_N = 0.4$ (grey).